


RESEARCH LETTER

Open Access



# Effects of topography and sea surface temperature anomalies on heavy rainfall induced by Typhoon Chaba in 2016

Woojin Cho<sup>1</sup>, Jinyoung Park<sup>1</sup>, Jihong Moon<sup>1</sup>, Dong-Hyun Cha<sup>1\*</sup> , Yu-min Moon<sup>2</sup>, Hyeon-Sung Kim<sup>3</sup>,  
Kyoung-jo Noh<sup>3</sup> and Sang-Hwan Park<sup>3</sup>

## Abstract

Typhoon Chaba made landfall on the Korean Peninsula in the fall of 2016, resulting in record-breaking rainfall in southeastern Korea. In particular, the Ulsan metropolitan region experienced the most severe floods due to heavy rainfall of 319 mm for just 3 h. The heavy rainfall was possibly associated with the mountainous southeastern Korea topography and the warm sea surface temperature (SST) anomaly in the East China Sea. In this study, the Weather Research and Forecasting (WRF) model was used to investigate the effects of topography and SST anomalies through high-resolution numerical experiments. Simulation using original topography showed more rainfall on the windward and less on the leeward slope compared to the experiment with reduced topography around Ulsan. The moist flow in the typhoon was raised by orographic uplift, enhancing precipitation on the windward side and summits of the mountains. The orographically induced updraft extended to the mid-troposphere and contributed to the upward vertical moisture flux associated with rainfall. Therefore, the mountainous topography around Ulsan affected the local change in rainfall induced by the simulated typhoon. In addition, SST on the track of the typhoon controlled storm intensity and caused extreme precipitation changes. The experiment using the original SST in the East China Sea simulated less decayed typhoons and produced more precipitation compared to the experiment wherein the positive SST anomaly in the East China Sea was removed. The warm SST anomaly hindered the weakening of the typhoon moving northward to the mid-latitudes. At landfall, the stronger typhoon contained more water vapor, transported more moisture inland, and generated increased precipitation.

**Keywords:** Typhoon-induced rainfall, Orographic uplift, Vertical moisture flux, Sea surface temperature anomaly

## Introduction

Typhoons, along with the intense precipitation associated with monsoons, are one of the most devastating weather disasters experienced on the Korean Peninsula. Destruction caused by typhoons includes structural damage by strong winds, coastal flooding by storm surges, and flash floods induced by torrential rains. However,

heavy rainfall is the most destructive weather phenomenon associated with typhoons. Typhoon Chaba (2016) was the fourth most intense typhoon to make landfall in South Korea in the fall season and caused intensified rainfall in the southeastern part of the Korean Peninsula. Typhoon Chaba resulted in seven casualties; the property damage amounted to 129 million USD. In particular, Ulsan located in the southeast of the country experienced severe flash floods due to record-breaking precipitation of more than 300 mm in a relatively short period of 3 h. The more severe effects of the typhoon experienced in Ulsan were attributed to the topographic effects of the

\*Correspondence: dhcha@unist.ac.kr

<sup>1</sup> Department of Urban and Environmental Engineering, Ulsan National Institute of Science and Technology, 50 UNIST-gil, Ulsu-gun, Ulsan 689-798, Republic of Korea

Full list of author information is available at the end of the article

mountainous terrain near the city, as well as the positive sea surface temperature (SST) anomaly of the East China Sea. Many previous studies have been conducted on these factors affecting typhoon rainfall.

Mountainous topography can increase typhoon-induced precipitation through mechanical air lifting and increasing orographic form drag; horizontal wind impinging on the windward slopes of mountains can generate an upward motion. Whether this upward motion passes over the mountain is determined by the wind speed perpendicular to the slopes, the moist static stability of the wind, and the height of the mountain (Chu and Lin 2000). If the orographic uplift is sufficiently strong to propel the air parcel to ascend above the level of free convection, instability increases and the air parcel continues to rise due to buoyancy. Therefore, moisture in the updraft can be condensed into cloud particles, and this orographically induced ascending motion generates favorable conditions for rainfall on the windward slope. In moist air systems such as typhoons, this process can occur more easily due to a low stability. In addition, a complex mountain range increases orographic form drag and causes the convergence of horizontal winds, which are also related to precipitation enhancement on mountains and can even deflect the path of typhoons (Lin et al. 2001; Witcraft et al. 2005; Tang and Chan 2014; Lee et al. 2018b).

To determine the specific conditions conducive to orographic rainfall, several studies analyzed topographic rainfall events using vertical profiles and reanalysis data and suggested common factors resulting in orographic rainfall: a high precipitation efficiency, a moist low-level jet, steep slopes, a conditionally or potentially unstable updraft, speed, and a horizontal scale of convective systems (Lin et al. 2001; Chiao and Lin 2003; Ming-Jen and Lin 2005; Witcraft et al. 2005; Lin 2007; Yang et al. 2008; Huang and Lin 2014; Lee et al. 2018b). Based on these factors required for orographic typhoon rainfall, Rostom (2015) and Agyakwah and Lin (2021) developed the Orographic Rainfall Index (ORI) and tested ORI for several tropical cyclones (TCs) using the Weather Research and Forecast (WRF) model. The ORI correlated well with the total rainfall.

To analyze the complex topographic effect using numerical experiments, a high-resolution grid spacing that can resolve mesoscale terrains is essential. Witcraft et al. (2005) reproduced heavy rainfall in Taiwan induced by Typhoon Bilis (2000) using the non-hydrostatic mesoscale model version 5 (MM5) with three domains and horizontal resolutions of 21, 7, and 2.33 km, respectively. Comparing the results of the three domains with different horizontal resolutions, a simulation with a 2.33-km grid

spacing showed the physical mechanisms responsible for orographic rainfall. A moist low-level jet associated with Typhoon Bilis impinged on the steep mountain range of Taiwan, and flow convergence in the upslope region generated a strong updraft and enhanced orographic rainfall.

Another lower boundary condition affecting typhoon-induced rainfall is the SST on the track of a typhoon. SST can change the intensity of typhoons and affects typhoon-induced rainfall. In general, the rainfall rate of typhoons tends to increase with typhoon intensity (Lin et al. 2015). Tao and Zhang (2014) found that TC intensity is significantly affected by SST, vertical wind shear, and mid-tropospheric relative humidity (RH). Large vertical wind shears tilt the structure of the TC, reducing diabatic heating release and hindering primary circulation of the TC by disrupting the development of vorticity in the mid-troposphere. Conversely, a warmer SST straightens the skewed vertical structure of the TC, increases resistance to unfavorable conditions, and increases diabatic heating near the TC center (Kanada et al. 2017). The lower-mid tropospheric RH in the tropics is also affected by SST. If the RH near the TC is reduced due to a lower SST, the convection in the TC center is weakened, and the TC size or TC rainfall area decreases with decreasing RH. Therefore, it has been proposed that the TC intensification is prompted by warmer SSTs underlying the TC.

In the past few decades, the SST and the low troposphere temperature of the western North Pacific (WNP) have increased rapidly because of climate change. These increases have led to enhanced typhoon intensity and changes in environmental conditions, such as synoptic fields (Emanuel 2005; Webster et al. 2005; Kim et al. 2011; Liu and Zhang 2013). In the early fall, the genesis points of typhoons in the WNP shift northward to the mid-latitudes, with a subsequent increase in track density. Moreover, an increasing SST over the WNP has resulted in a decreasing vertical wind shear over the mid-latitude region, creating favorable conditions for the movement of typhoons northward to South Korea and Japan (Lee et al. 2019).

There have been several studies on Typhoon Chaba analyzing the storm intensity, storm surge, and rainfall with radar observation and weather forecast and ocean wave models (Jang et al. 2018; Kim et al. 2018; Yuk and Joh 2019; Do and Kim 2021). However, the reason for the heavy rainfall in Ulsan caused by Typhoon Chaba has not been examined. Therefore, in this study, we investigate the effects of orography and SST on heavy rainfall induced by Typhoon Chaba through numerical experiments using the WRF model. "Methods and experiment design" section describes the design and applications of

numerical experiments. "Results and discussion" section presents the results of our experiments and discusses the topographic effects and influence of SST on the precipitation of Typhoon Chaba. Finally, the conclusions and scope for future research are presented in "Summary and conclusion" section.

**Methods and experiment design**

The WRF model version 4.2.0, which can reproduce mesoscale weather features with a high resolution, was used for all simulations. The horizontal grid spacing (grid points) of each domain was 9 km (550 × 660), 3 km

(490 × 871), and 1 km (250 × 250) for the first (D01), second (D02), and third (D03) domains, respectively, which were all fixed in this study. All domains contained ten grids as boundary buffer zones. D01 contained the East Asia region and part of the western Pacific. To resolve the inner-core structure and intensification of Typhoon Chaba, the southern boundary of D02 was set to 20°N. A 1-km high-resolution domain (D03) located in the southeastern area of the Korean Peninsula was used to capture the topography near Ulsan, and the result of D03 was used to analyze typhoon-induced rainfall (Fig. 1). The one-way nesting method was applied to all experiments.

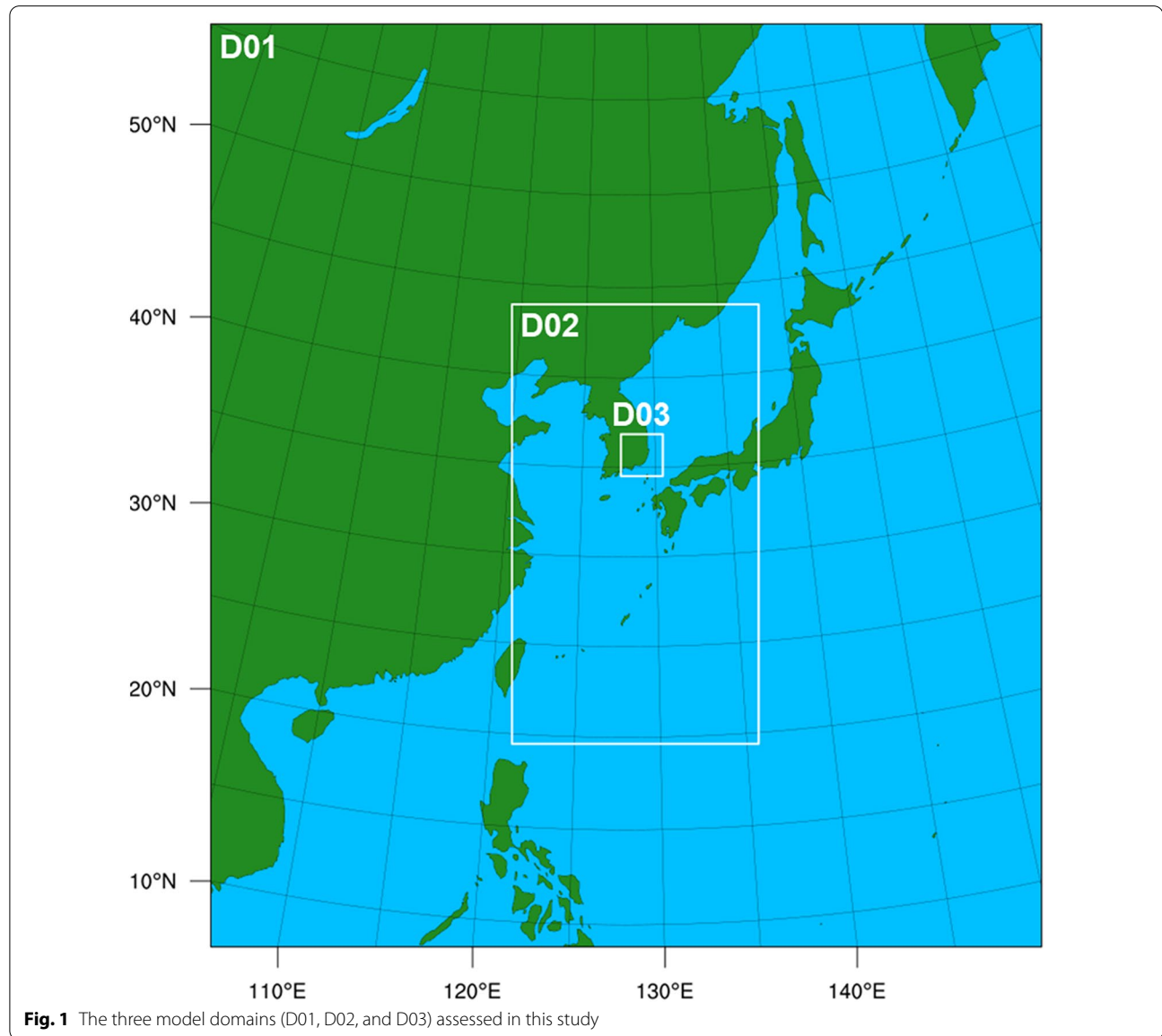


**Fig. 1** The three model domains (D01, D02, and D03) assessed in this study

**Table 1** Model configuration

Prototype	WRF V4.2.0		
Initial/boundary condition	FNL (6-hourly 0.25° × 0.25°)		
Lower Boundary condition	OISST v2.0 (daily mean SST 0.25° × 0.25°)		
Domains	D01	D02	D03
Resolution	9 km	3 km	1 km
Dimension	550 × 660	490 × 871	250 × 250
Nesting	1-way nesting		
Microphysics scheme	P3		
Cumulus scheme	KF	X	X
PBL scheme	YSU		
Longwave/shortwave radiation scheme	RRTM/Dudhia		
Spectral nudging	O	X	X

The vertical coordinate was a hybrid sigma-pressure coordinate with 35 levels. All simulations were integrated for 120 h at 0000 UTC on October 1, 2016.

As shown in Table 1, the National Centers for Environment Prediction (NCEP) final analysis (FNL) with a resolution of 0.25° × 0.25° latitude–longitude dataset was used for the initial and lateral boundary conditions. National Oceanic and Atmospheric Administration (NOAA) Optimum Interpolation Sea Surface Temperature (OISST) version 2.0 data were employed as the lower boundary condition for the WRF runs. The predicted particle properties (P3) scheme (Morrison and Milbrandt 2015; Morrison et al. 2015; Milbrandt and Morrison 2016) for grid-scale cloud microphysics and the YSU scheme (Hong et al. 2006; Hong 2010) for planetary boundary parameterization were used for all three domains, and the Kain–Fritsch cumulus parameterization scheme (Kain and Fritsch 1990; Kain et al. 2003; Kain 2004) was used at D01 only to capture the sub-grid scale convection.

Simulating typhoon rainfall is one of the challenges in weather forecasting owing to uncertainty in the prediction of typhoon tracks and intensities. Moreover, precipitation induced by typhoons is considerably sensitive to typhoon tracks. Therefore, we also applied the spectral nudging method (von Storch et al. 2000) to D01 to reproduce the typhoon tracks realistically, using the optimized options as in Moon et al. (2018) (Table 1).

Four numerical experiments were conducted to investigate the effects of topography and SST on heavy precipitation at the landfall of Typhoon Chaba. First, a control experiment (CTL) was performed to examine whether the WRF model simulates Typhoon Chaba realistically compared to the Joint Typhoon Warning Center (JTWC) best track data and the accumulated precipitation data of the Automatic Weather Station (AWS) and Automated Surface Observing System (ASOS). An experiment with reduced topography around Ulsan was denoted as TOPO; the terrain height above 300 m within 35°00′ N to 35°57′ N and 128°48′ E to 130°00′ E in TOPO was decreased to half of the original elevation. The maximum height difference between CTL and TOPO exceeded 500 m on the western mountainside of Ulsan. Lowered fields were smoothed to reduce the large gradient of terrain caused by a lowered height; this area was used to analyze signals of orographically enhanced precipitation at the landfall of Typhoon Chaba (Fig. 2).

Climatological SST data from 1982 to 2018 were created using OISST daily mean data; the SST in the WNP was higher than the climatological SST in early October 2016. The SST of the East China Sea and the adjacent ocean of Japan during the simulation period was 1.0 °C higher than the climatological SST (Fig. 3). In particular, the SST in the East China Sea during the experiment period was 2.0 °C higher under the track of Typhoon Chaba and it was second highest between 1982 and 2018, exceeding one standard deviation (Additional file 1: Fig. S2). This positive SST anomaly may have affected the strength of Typhoon Chaba and the intensity of rainfall at landfall; therefore, we conducted a positive anomaly removal experiment (CSST). The positive SST anomaly value in the blue box at D02 was eliminated in the CSST. Additionally, we conducted a fourth experiment (CSST\_TOPO) by merging the CSST and TOPO experiments to investigate the combined impacts of topography and the positive SST anomaly on typhoon-induced rainfall.

**Results and discussion**

**Simulated typhoon track and intensity**

The simulated typhoons in the high-resolution D02 domain were tracked using a simple method to identify the minimum value in the sea level pressure field. All simulated typhoons entered D02 at 0000 UTC on October 2, 2016 and then intensified. The tracking started

(See figure on next page.)

**Fig. 2** Topography of D03 and height difference (m) between CTL and TOPO. Ulsan is indicated by the black box. **a** Terrain height (m) of CTL experiment and **b** height difference (m) between CTL and TOPO

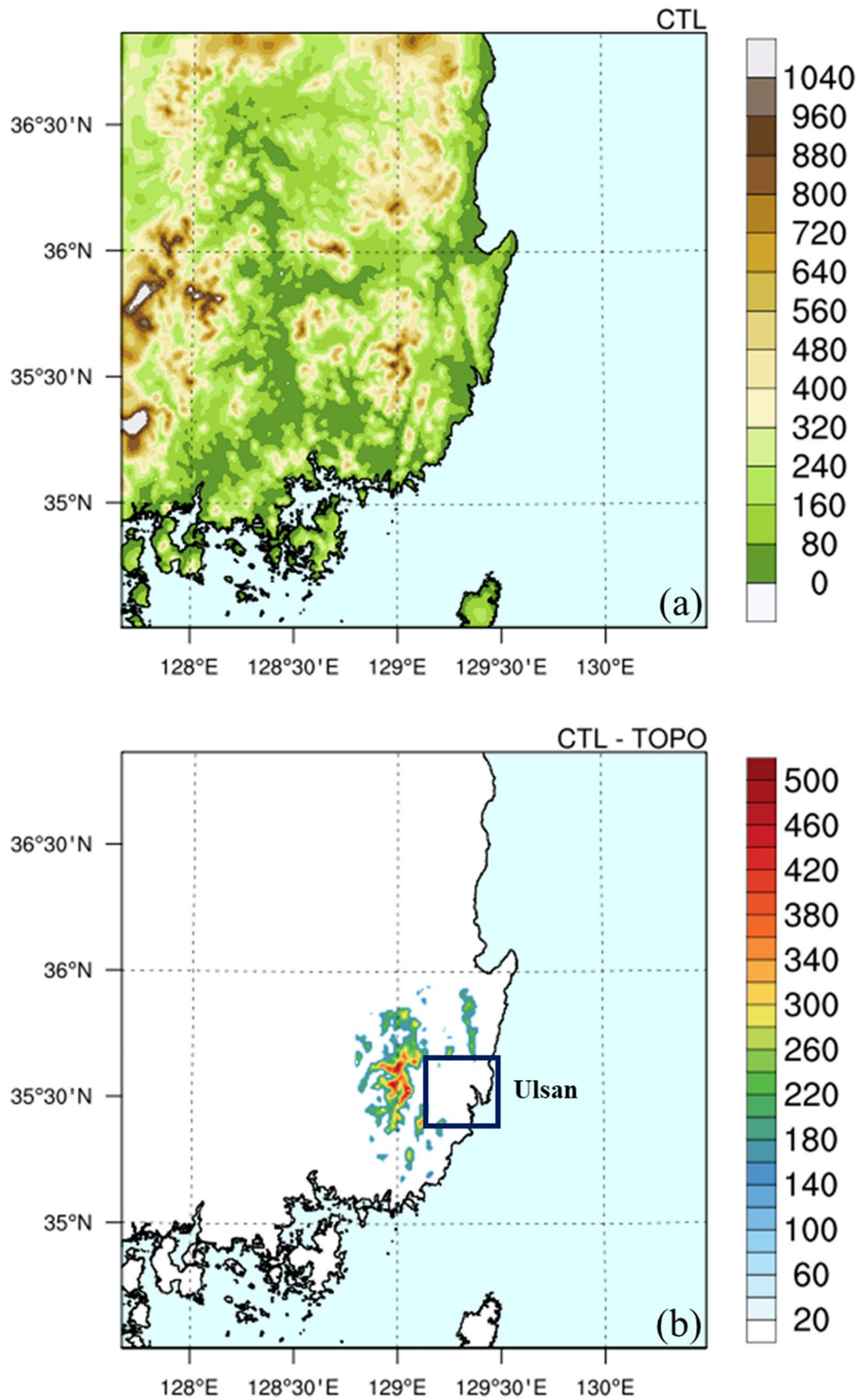
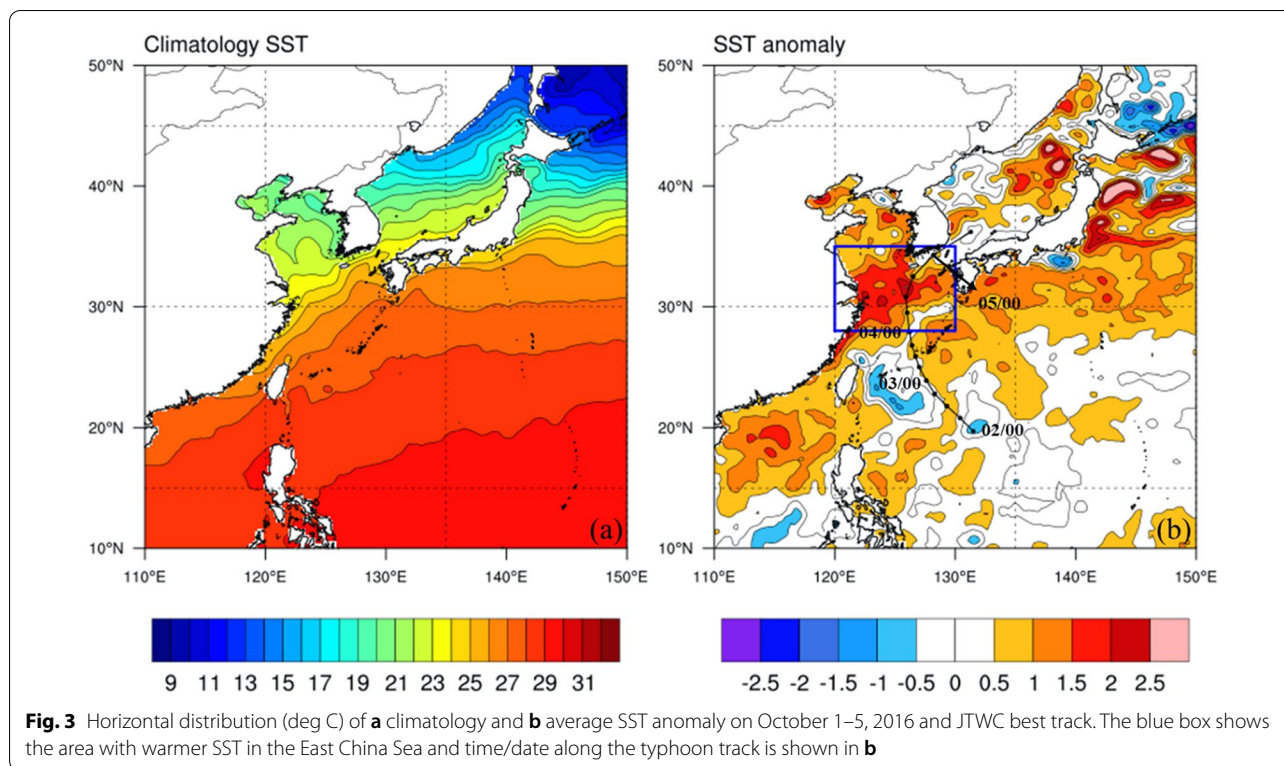


**Fig. 2** (See legend on previous page.)



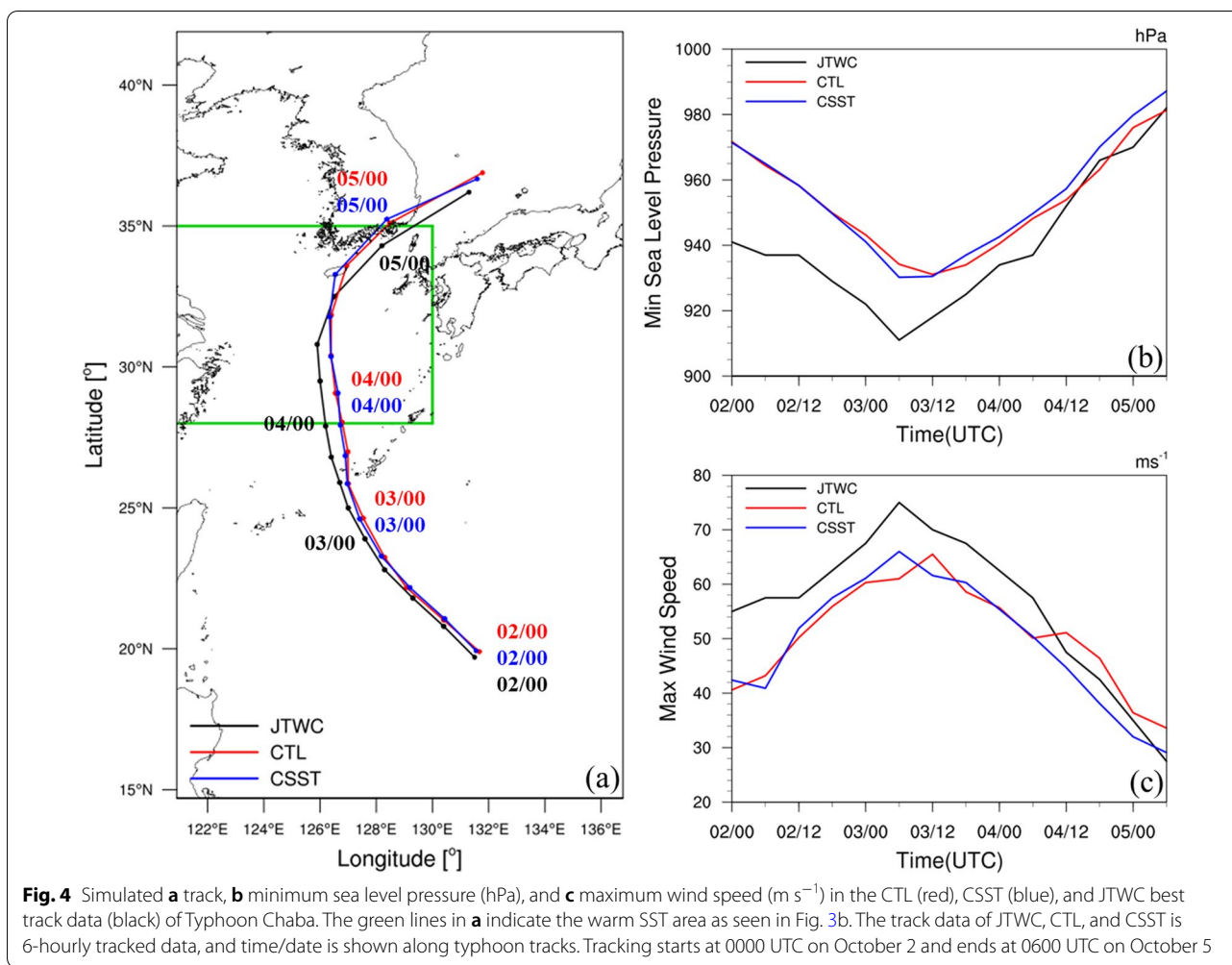
at 0000 UTC on October 2 and ended at 0600 UTC on October 5, when the typhoons passed South Korea and dissipated (Fig. 4). The typhoon tracks simulated in all experiments were comparable to the JTWC best track data. Employing the spectral nudging method, the large-scale fields simulated by the WRF model were close to the FNL analysis; therefore, the typhoon tracks were realistically reproduced in the 5-day runs, which is consistent with Moon et al. (2018). The tracks of CTL and CSST were similar before 1200 UTC on October 4, and subsequently shifted eastward (Fig. 4a). After 1800 UTC on October 4, both CTL and CSST simulated a slightly northward shifted track relative to the JTWC indicating landfall, while the JTWC best track passed through the Korean Strait.

Both CTL and CSST underestimated the typhoon intensity compared to JTWC. However, two experiments reasonably captured the intensification and peak time of Typhoon Chaba with a similar maximum intensity. After passing Okinawa Island and the East China Sea, all simulated typhoons weakened due to the lower SST of this area (see Fig. 3a). However, in CTL, the strength of the typhoon did not continue to decrease but the intensity

was maintained, unlike in CSST (Fig. 4c). The difference in the typhoon intensity between these experiments may have been caused by SST anomalies in the East China Sea. Overall, TOPO and CSST\_TOPO showed almost the same typhoon tracks and intensities as CTL and CSST, respectively (not shown).

### Accumulated precipitation induced by Typhoon Chaba

The 24-h accumulated precipitation of the observation (AWS and ASOS) and experiments is shown in Fig. 5. As shown in Fig. 4, the center of the simulated typhoons crossed the archipelago on the southwestern side of D03 and passed over the mountain range west of Ulsan, while the JTWC best track was shifted further southward in the sea. Although Ulsan was not the closest location to the typhoon center, the maximum accumulated rainfall occurred at Ulsan. The observation indicated more than 200 mm of rainfall around Ulsan; more than 300 mm rainfall was observed in the mountains southwest of Ulsan and southern part of the mountain range north of Ulsan (Fig. 5a). This extreme rainfall amount



of observation implied that a local source near Ulsan affected the heavy rainfall event induced by Typhoon Chaba. The rainfall area of all simulations was shifted somewhat northward, and the rainfall amount in Ulsan was underestimated because of the northward shift of the typhoon tracks in the numerical experiments. However, CTL captured more than 200 mm of heavy rainfall, in which the affected area was wider than that in CSST

(Fig. 5b, c). The rainfall peak in CTL was located in the northern part of the mountains west and north of Ulsan, and its amount exceeded 340 mm, similar to the maximum rainfall of the observation; however, in CSST, the heavy rainfall area ( $35^{\circ}30' N$  to  $36^{\circ}00' N$  and  $129^{\circ}00' E$  to  $129^{\circ}30' E$ ) was smaller than in CTL, and the peak rainfall was less than 260 mm.

(See figure on next page.)

**Fig. 5** Horizontal distribution of accumulated precipitation ( $mm day^{-1}$ , shading) in **a** observation, **b** CTL, and **c** CSST. Accumulated rainfall difference ( $mm day^{-1}$ , shading) between **d** CTL and TOPO, **e** CSST and CSST\_TOPO, and **f** CTL and CSST. The black contour lines in **a-f** show the height difference (m, contour with 60 m interval) between CTL and TOPO, indicating mountain ranges near Ulsan. The gray dots in **a** show the locations of observation stations

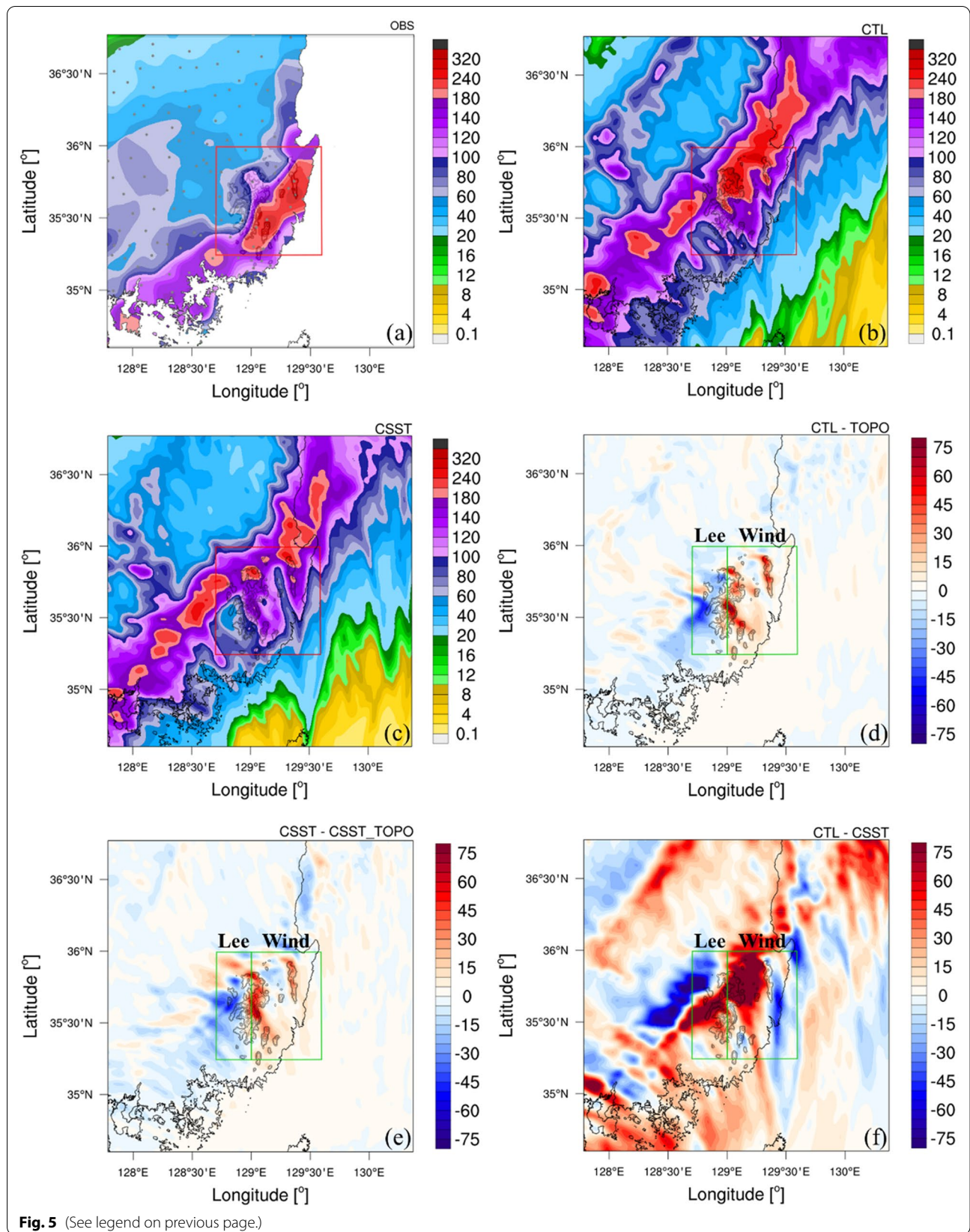


**Fig. 5** (See legend on previous page.)



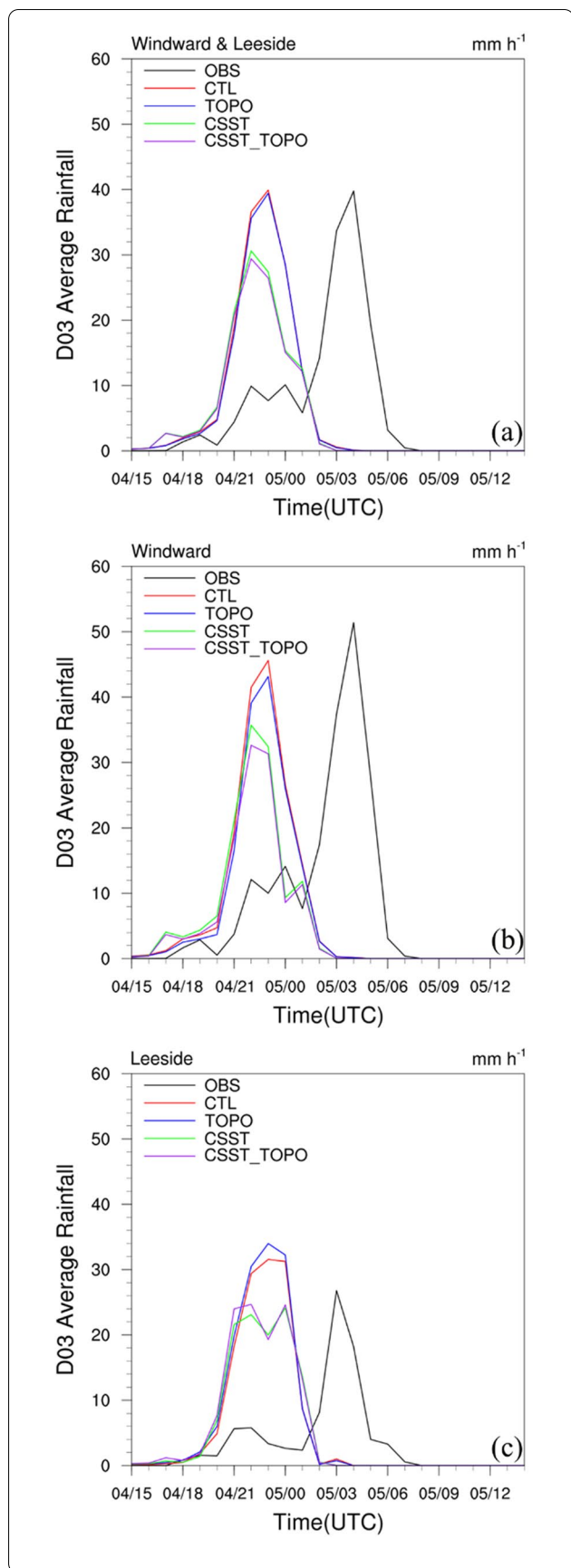


**Fig. 6** Time series of average rainfall (mm h<sup>-1</sup>) in the observation (black), CTL (red), TOPO (blue), CSST (green), and CSST\_TOPO (purple) in the **a** windward and leaside, **b** windward, and **c** leaside

The distribution of the precipitation difference between CTL and the TOPO was divided into two areas (Fig. 5d). Considering the counterclockwise circulation of the typhoon, we divided the red box in Fig. 5a, b, and c into a windward and leeward side, indicated by the green box in Fig. 5d and e. The experiments with original topography (i.e., CTL and CSST) simulated more rainfall on the windward slope of the mountain range and less rainfall on the leeward side. Conversely, the experiments with reduced topography (i.e., TOPO and CSST\_TOPO) showed less rainfall on the windward side and increased rainfall on the leeward side. This signal was clearer on the mountain range west of Ulsan than on the mountain range north of Ulsan. Additionally, Fig. 5f shows that CTL simulated more precipitation in the area of interest than CSST, although the tracks of the simulated typhoons between CTL and CSST were not exactly the same.

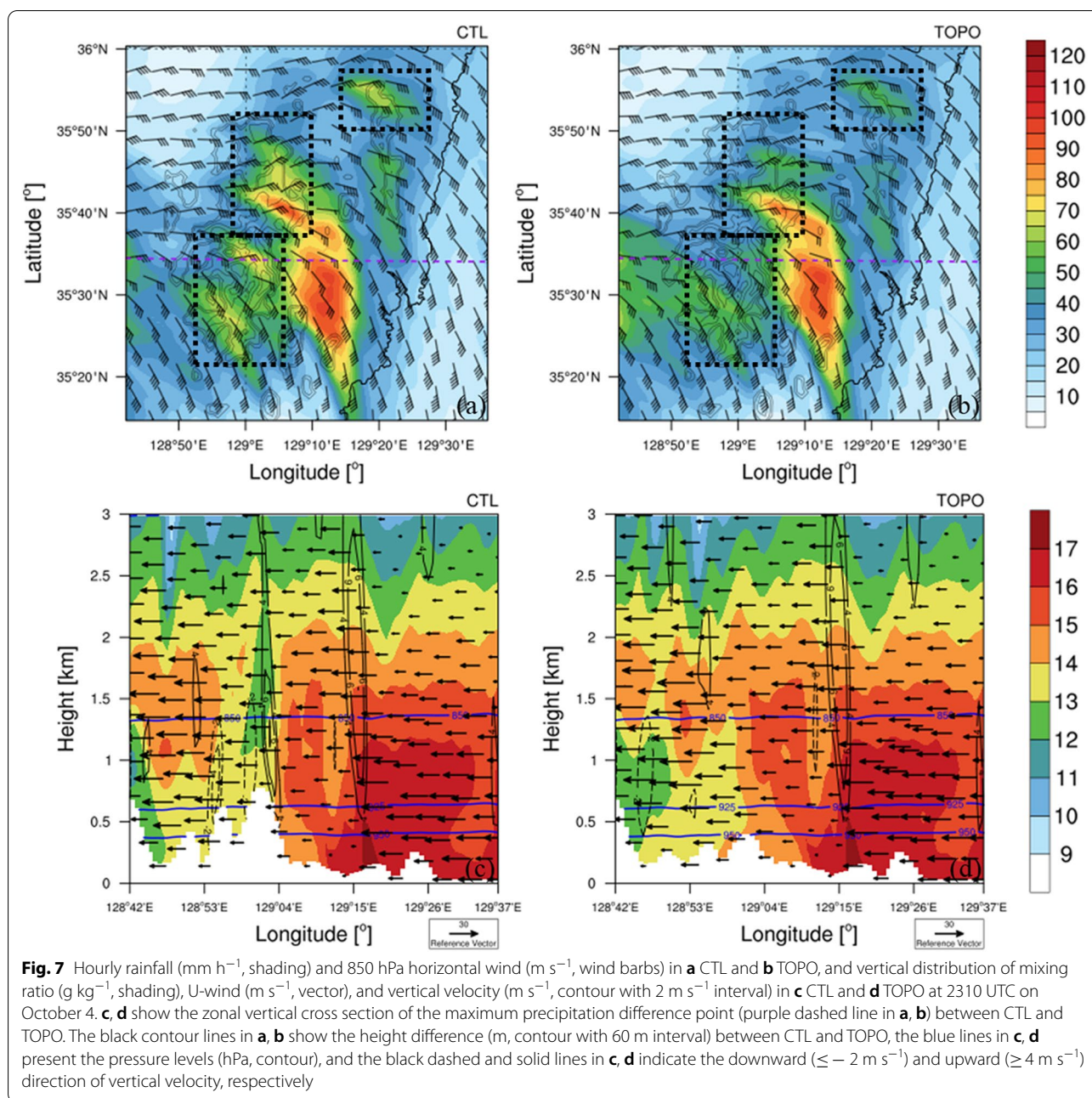
These results were confirmed by checking the time series of the spatial mean rain rate for each area (Fig. 6). All experiments simulated the heavy rainfall 6 h earlier than the observation, and the peaks of hourly rainfall for both the windward and leeward side were similar between

**Table 2** 24-h accumulated rainfall (mm) averaged for windward and leeward, windward, and leeward

	Windward and leeward	Windward	Leeward
OBS (mm)	153.23	190.11	84.71
CTL (mm)	149.58	164.09	128.19
TOPO (mm)	146.11	152.97	136.03
CSST (mm)	123.70	130.87	113.15
CSST_TOPO (mm)	119.65	120.51	118.41

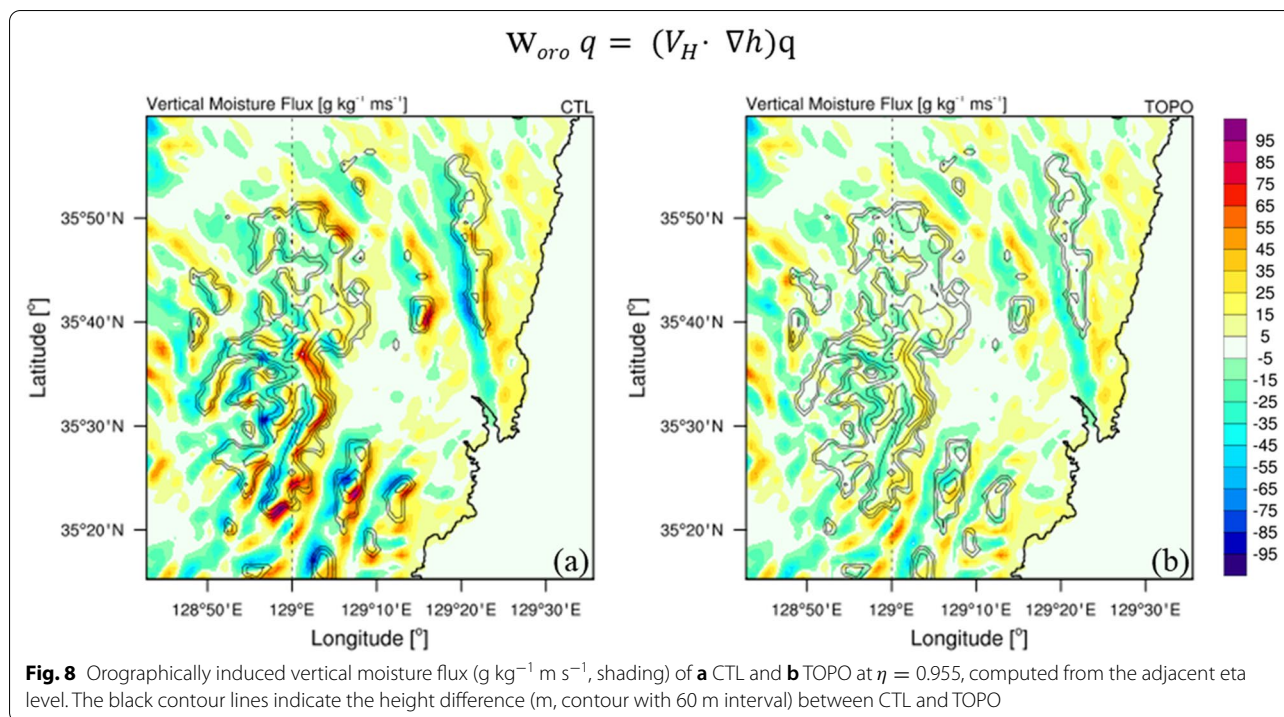
**Table 3** Percentile of accumulated precipitation difference between experiments for windward and leeward, windward, and leeward. The percentile denominator is a subtraction term

	Windward and leeward	Windward	Leeward
TOPO-CTL (%)	- 2.32	- 6.79	6.11
CSST-CTL (%)	- 17.29	- 20.27	- 11.67
CSST_TOPO-CTL (%)	- 19.99	- 26.57	- 7.55
CSST_TOPO-CSST (%)	- 3.26	- 7.91	4.66



the observation and CTL. The total rainfall averaged for both areas in the observation and CTL were 153.23 mm and 149.58 mm, respectively (Table 2). The observation showed more (less) rainfall on the windward side (lee-side) than CTL. The total precipitation of both areas for CTL and TOPO was also similar, but CTL produced

more rainfall on the windward side and less on the lee-side, which is consistent with Fig. 5d. The comparison between CSST and CSST\_TOPO yielded the same result. However, CSST and CSST\_TOPO produced less rainfall in all areas than CTL and TOPO, respectively, and may be associated with the simulated typhoon intensity.



To determine the quantitative difference in precipitation, the percentile of the accumulated rainfall difference between each experiment was calculated. From Table 3, the rainfall on the windward side of CTL was by 6.79% higher than that of TOPO, while TOPO simulated a by 6.11% higher precipitation over the leeside than CTL. Similarly, CSST simulated 7.91% more rainfall on the windward side and 4.66% less rainfall on the leeward side than CSST\_TOPO. However, CSST and CSST\_TOPO reproduced 17.29% and 19.99% less rainfall, respectively, in both areas compared to CTL, and the difference was more significant on the windward side. To sum up, the CTL experiment reproduced a typhoon-induced precipitation comparable to the observation, whereas the TOPO, CSST, and CSST\_TOPO experiments simulated less rainfall than CTL. In particular, a decreasing precipitation amount was most often simulated in CSST\_TOPO, which included the combined effects of a reduced topography around Ulsan and a decreased SST over the East China Sea. These results indicate that the heavy rainfall induced by the Typhoon Chaba could be affected by the mountainous topography as well as the SST anomaly. In addition, no matter whether the simulated typhoon intensity was strong or weak, the change in precipitation

on the mountain slope due to topographic effects was evident.

### Topographic effect on typhoon-induced rainfall

To investigate the topographic effect on heavy rainfall in Ulsan, the results of the CTL and TOPO experiments were compared. Even though the simulated typhoon track and rainfall distribution did not match the JTWC best track and the observations, the topographic effect appeared in the comparison of the CTL and TOPO simulations (Fig. 7a, b). The horizontal wind at 850 hPa decelerated over Ulsan in both CTL and TOPO due to orographic form drag. This deceleration led to low-level convergence and convection on the east of the mountain range. However, the low-level wind in TOPO was less decreased than that in CTL; therefore, the torrential precipitation on the mountain slopes (within the black dashed line box where the difference in hourly rainfall between CTL and TOPO is large in Fig. 7a, b) was slightly reduced in TOPO. In the zonal vertical cross section of the purple dashed line in Fig. 7a and b, which shows the maximum difference in the precipitation between CTL and TOPO, an upward motion appeared

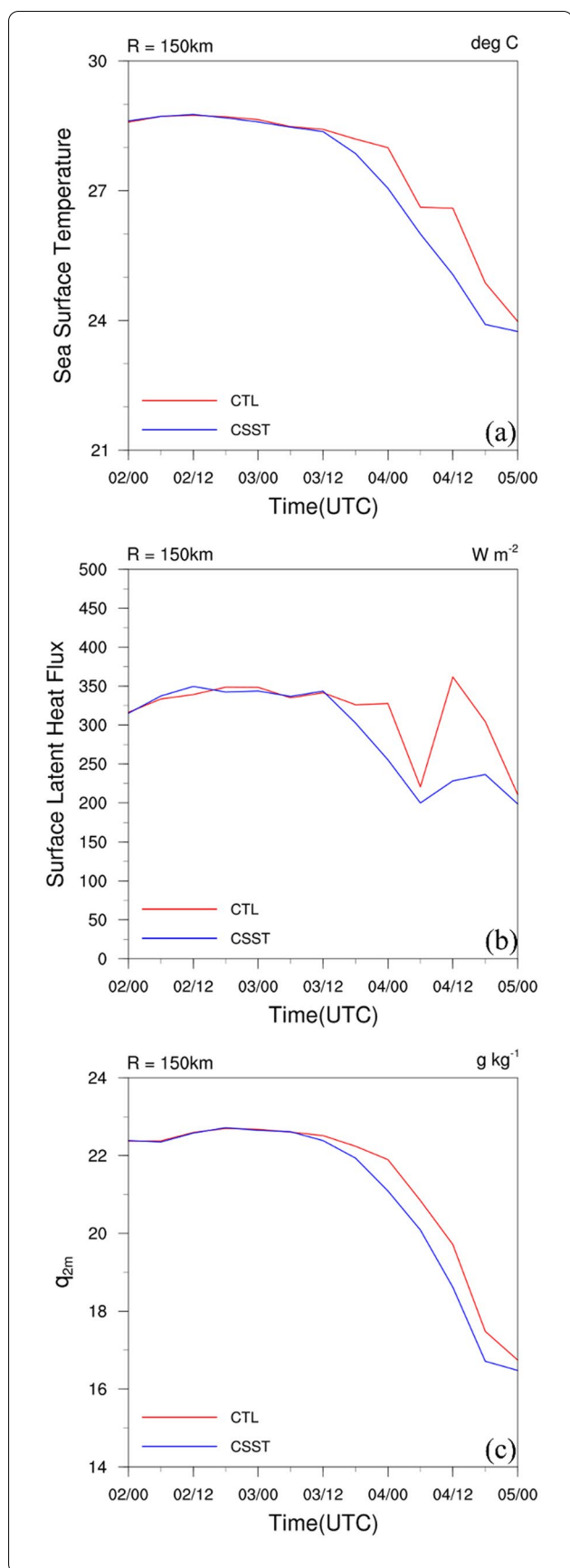


**Fig. 9** Time series of average **a** SST (deg C), **b** SLHF ( $\text{W m}^{-2}$ ), and **c** 2 m water vapor ( $\text{g kg}^{-1}$ ) around the typhoon's center in CTL (red) and CSST (blue)

on the windward slope from the surface to the upper level in CTL (Fig. 7c); a downward motion was also evident on the leeward side. Additionally, the stream of water vapor over the windward side in CTL was disconnected because the orographically induced enhancement of rainfall and convection led to the consumption of water vapor (Fig. 7c, d). However, the horizontal wind in TOPO passed smoothly, and no vertical motion appeared (Fig. 7d).

The enhanced convection on the windward slope transported more water vapor upward, and this could be shown as vertical moisture flux. The orographically induced vertical moisture flux could be expressed by multiplying the water vapor mixing ratio and orographic updraft, which was written as an inner product of the horizontal wind and gradient of terrain heights (Lin et al. 2001). Figure 8 shows the orographically induced vertical moisture flux in CTL and TOPO. Similar to Witcraft et al (2005), the orographically induced vertical moisture flux was calculated at  $\eta = 0.955$  in the WRF simulations. In CTL, upward vertical moisture flux was dominant on the windward slope; downward vertical moisture flux appeared on the leeside. However, no significant signals were captured in TOPO. This means that the mountainous topography around Ulsan increased orographically induced vertical moisture flux on the windward side, which contributed to enhanced precipitation. Through TOPO, therefore, it was confirmed that the typhoon-induced heavy rainfall was possible because of Ulsan's unique orography effect.

### Effect of SST on Typhoon Chaba

Numerous researchers have established the correlation between SST and typhoon intensity, whereby a warmer SST contributes to maintaining typhoon intensity during the transition to the mid-latitudes. When typhoons maintain their intensity due to warmer SSTs, the possibility of stronger typhoons making landfall can increase (Park et al. 2011). Typhoon Chaba (2016) can be an example of typhoons that experienced an increase in intensity due to a warmer SST. The typhoon passed over the positive SST anomaly in the East China Sea from 1200 to 1800 UTC on October 4 (Fig. 3b). This positive SST anomaly hindered the weakening of the typhoon, as seen in the JTWC best track data (Fig. 4b, c). To examine the effect of the warm SST anomaly in the East China Sea, we compared the results between CTL and CSST. Figure 9 shows

the time series of the SST, surface latent heat flux (SLHF), and water vapor at 2 m above the surface in D02 averaged within a radius of 150 km from the typhoon center. Until 1200 UTC on October 3, both the SST and SLHF were approximately the same. However, after 1200 UTC, the typhoon in CSST passed over the East China Sea, and the SST continued to decrease until the typhoon made landfall. However, in CTL, the SST slowly decreased and remained at 26 °C from 0600 to 1200 UTC on October 4 (Fig. 9a). Moreover, the intensity of the simulated typhoon in CTL marginally increased with the SST trend when it passed through the warmer SST in the East China Sea (from 0600 to 1200 UTC on October 4). After that, the difference in the typhoon intensity between CTL and CSST lasted before dissipation.

The SLHF on the ocean is affected by the SST, wind speed, and the vertical moisture gradient, and calculated using the following bulk formula with these variables.  $w$

$$LHF = \rho L_v C_h W_s \Delta q,$$

where  $\rho$  is the air density ( $\text{kg m}^{-3}$ ),  $L_v$  is the latent heat of vaporization ( $2.44 \times 10^6 \text{ J kg}^{-1}$ ),  $C_h$  is the transfer coefficient ( $1.3 \times 10^{-3}$ ),  $W_s$  is the 10-m wind speed, and  $\Delta q = (q_s - q_{2m})$  is the moisture gradient between the sea surface and the air 2 m above it (Kumar et al. 2017).

The simulated typhoons entered the dry area in the mid-latitude after 1200 UTC on October 3, and then, the SST, wind speed, and  $q_{2m}$  started to decrease in both CTL and CSST (Figs. 4, 9). The SLHF in CSST decreased after 1200 UTC on October 3, while the decreasing SLHF in CTL was prominent after 0000 UTC on October 4 when the SST cooled notably (Fig. 9a, b). At 1200 UTC on October 4, the SST of CTL was similar to that at 0600 UTC on October 4 and  $q_s$  did not change much due to this similar SST. However, the wind speed increased and  $q_{2m}$  considerably decreased (Figs. 4, 9). Therefore, SLHF drastically increased at 1200 UTC due to the enhanced  $W_s$  and the increased  $\Delta q$  in the bulk formula. However, the SST, wind speed, and  $q_{2m}$  in CSST decreased continuously, so a minor increase in the SLHF appeared at 1200 UTC. After leaving the area with warm SST, the SLHF in CTL decreased, and the typhoon also weakened.

The maximum difference in typhoon intensity between CTL and CSST appeared at 1200 UTC on October 4;

the vertical structure of the typhoon in CTL and CSST at this time is shown in Fig. 10. Entering the upper-level westerly wind region in the mid-latitudes, the typhoon in both experiments tilted eastward, but the eye and eyewall were clearly visible. The maximum wind speed recorded in CTL and CSST was at 900 hPa, and the horizontal wind speed in CTL exceeded  $70 \text{ m s}^{-1}$  (Fig. 10a). However, CSST indicated a maximum wind speed of less than  $65 \text{ m s}^{-1}$  (Fig. 10b). In addition, the azimuthally averaged tangential wind for both experiments recorded a maximum pressure at 900 hPa; CTL showed stronger tangential winds than the CSST (Fig. 10c, d). For the radial wind of the typhoon, CTL simulated a stronger low-level inflow and upper-level outflow, as well as a wider outflow than the CSST (Fig. 10e, f). These results indicate that the low-level convergence and upper-level divergence were stronger in CTL, and the secondary circulation of the typhoon was more powerful. Similar to previous studies (Tao and Zhang 2014; Sun et al. 2017; Li and Huang 2018), our results indicate that a warm SST in typhoon tracks could play an important role in maintaining the strength of typhoons during their dissipation in the mid-latitudes.

The change in typhoon intensity due to SST can affect moisture transport; hence, precipitation changes with typhoon intensity (Lin et al. 2015). This trend was indicated by the accumulated rainfall for the study area displayed in Figs. 5 and 6. The low-level moisture distribution of CTL and CSST at 0000 UTC on October 5 showed that moisture transport was associated with changes in typhoon intensity and SST (Fig. 11). The center of the typhoon in both experiments was located on the southwestern coast of Ulsan, and a mass of moisture covered the typhoon center. Dry air penetrated the west side of the typhoon and wrapped around the typhoon center. On the east side of the typhoon center, moisture was transported from the ocean to the land by cyclonic circulation. This moisture channel in CTL was more significant and evident because the simulated typhoon in CTL had a stronger intensity and more substantial structure than in CSST (Figs. 4b, 10, 11a). However, in CSST, the moisture transport was weaker and the air surrounding the simulated typhoon core was drier, especially in the northwest of the typhoon center. The dry air

(See figure on next page.)

**Fig. 10** Vertical structures of simulated typhoon at 1200 UTC on October 4. Horizontal wind (shading,  $\text{m s}^{-1}$ ) and potential temperature (contour, K with 5 K interval) in **a** CTL and **b** CSST, tangential wind ( $\text{m s}^{-1}$ ) in **c** CTL and **d** CSST, and radial wind ( $\text{m s}^{-1}$ ) in **e** CTL and **f** CSST

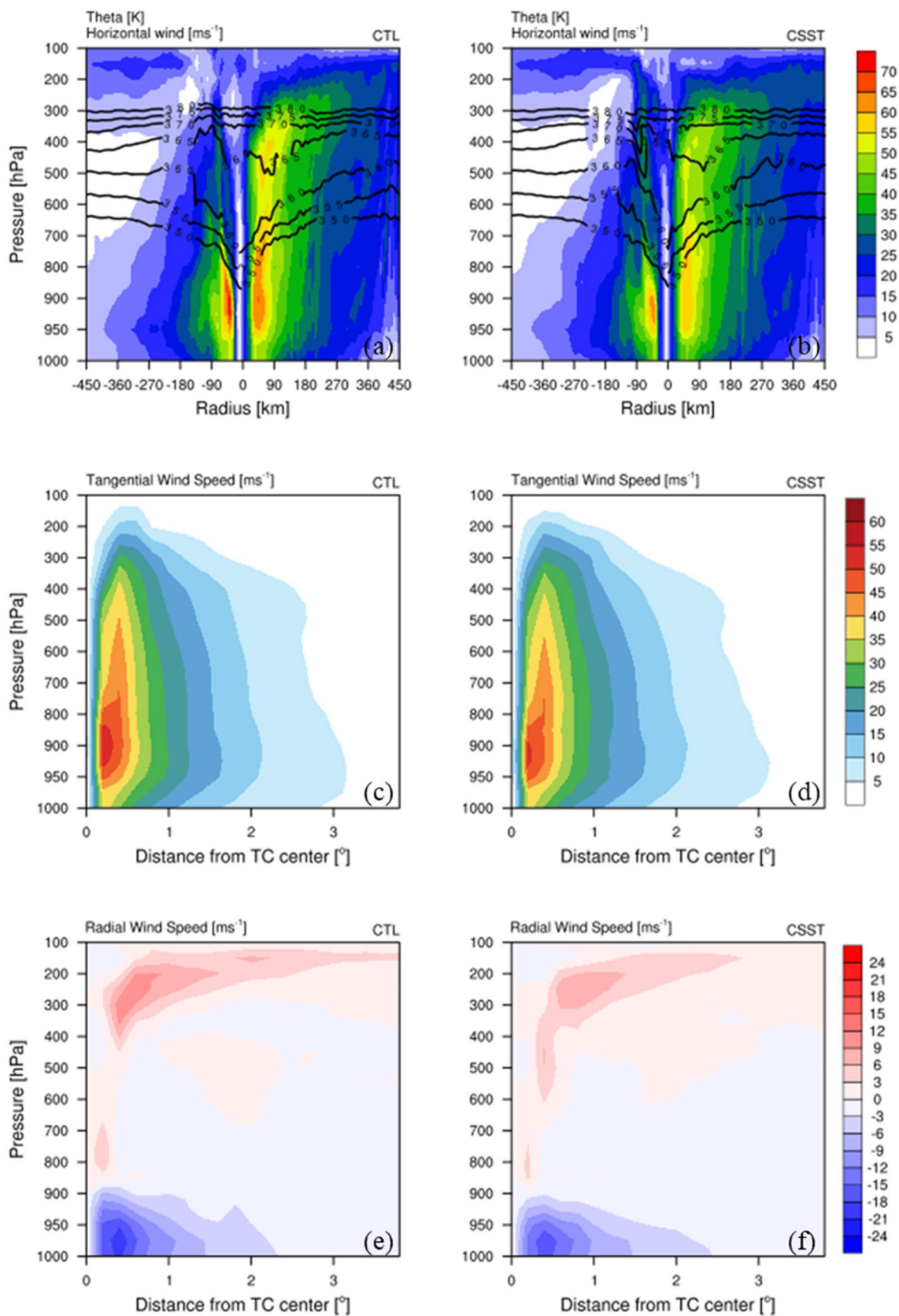


Fig. 10 (See legend on previous page.)

intrusion was stronger in CSST than in CTL and cut off the moisture connection with the center (Fig. 11b). We also calculated the differences in water vapor and precipitable water amounts between CTL and CSST (Fig. 11c), which flowed into the Ulsan region (blue box in Fig. 11a, b) by cyclonic circulation of Typhoon Chaba. The CTL experiment with a stronger typhoon tended to simulate a higher moisture transport. In particular, the maximum difference in the two variables between CTL and CSST appeared before heavy rainfall started. This implies that the stronger typhoon enhanced by a warmer SST conveys more moisture to the land, which leads to heavy rainfall inland.

### Summary and conclusion

Typhoon Chaba, which occurred during the boreal fall season in 2016, made landfall on the Korean Peninsula and caused record-breaking rainfall in Ulsan due to the effects of the local topography and the positive SST anomalies of the East China Sea on the typhoon-induced precipitation. In this study, we examined both topography and SST effects on the torrential rainfall associated with Typhoon Chaba through sensitivity experiments using the WRF model.

In our simulations, CTL showed a strong orographic updraft on the windward slope, which extended to the mid-troposphere region. However, this upward motion on the height-reduced mountain slope was not indicated in TOPO with reduced topography. Therefore, on the windward side, CTL simulated more precipitation than TOPO owing to topography-induced updraft. However, on the leeside, downward motion of air parcels was reproduced in CTL, and the rainfall amount in this experiment was lower than that in TOPO, indicating that the topography around Ulsan could affect local changes in typhoon-induced rainfall. Therefore, a high-resolution model that can resolve mesoscale mountain ranges is required to reasonably predict orographic heavy rainfall related to typhoons.

Typhoon Chaba also passed through the East China Sea with a warm SST anomaly. Therefore, the average SST along the typhoon track in CTL with a normal SST slowly decreased and remained at 26 °C for 6 h, while the typhoon's intensity simultaneously increased. However, in the CSST simulation with climatological SST, the SST

and typhoon intensity continued to decrease before the typhoon made landfall. Thus, a comparison of the CTL and CSST simulations showed that the slight intensification of the typhoon due to a warm SST anomaly caused a difference in the intensity of the landfalling typhoon. This difference also altered the water vapor content of the typhoon and affected the amount of moisture transported inland. Therefore, the stronger typhoon transported more water vapor inland and generated enhanced precipitation.

We showed that the impacts of topography and SST on typhoon-induced heavy rainfall over the Korean Peninsula are significant, indicating the importance of these factors in local heavy rainfall forecasts. Therefore, a very high-resolution (about 1 km horizontal grid spacing) numerical model as well as more detailed topography data are needed to reasonably simulate the impact of topography on typhoon-induced heavy rainfall. In addition, the uncertainty of SST data in the East China Sea and the Yellow Sea is considerable due to the low density of in situ observation (e.g., ARGO), as mentioned in Lee et al. (2018a). Therefore, more accurate SST data in these regions are required to improve typhoon and associated precipitation forecasts. Moreover, the effect of topography on heavy rainfall by Typhoon Chaba might be somewhat overestimated because the track of the simulated typhoon was shifted northward as compared to the best track, inducing the northward migration of the precipitation zone to the mountainous regions as shown in Fig. 5b, c. Therefore, improvements of simulated TC tracks are further needed to quantitatively investigate topography effects on typhoon-induced heavy rainfall.

This study identified the effects of topography and a warm SST in the East China Sea on heavy rainfall induced by Typhoon Chaba through the TOPO experiment with a reduced terrain and the CSST experiment with a climatological SST. Further sensitivity tests to varying terrain height and SST anomalies in the East China Sea are required to quantitatively interpret the effects of these two conditions and to understand other physical factors (i.e., moisture contents, instability, and convective systems). In addition, additional experiments on other typhoons similar to Typhoon Chaba are required to generalize our results. Furthermore, the relationship between a warm SST in the East China Sea and the change in typhoon activity around the Korean Peninsula needs to be investigated to improve typhoon forecasting.

(See figure on next page.)

**Fig. 11** Horizontal distribution of 850 hPa water vapor ( $\text{g kg}^{-1}$ ) in **a** CTL and **b** CSST at 0000 UTC on October 5, and **c** time series of difference in water vapor ( $\text{g kg}^{-1}$ ) and precipitable water ( $\text{kg m}^{-2}$ ) between CTL and CSST within the blue box in the **a, b**

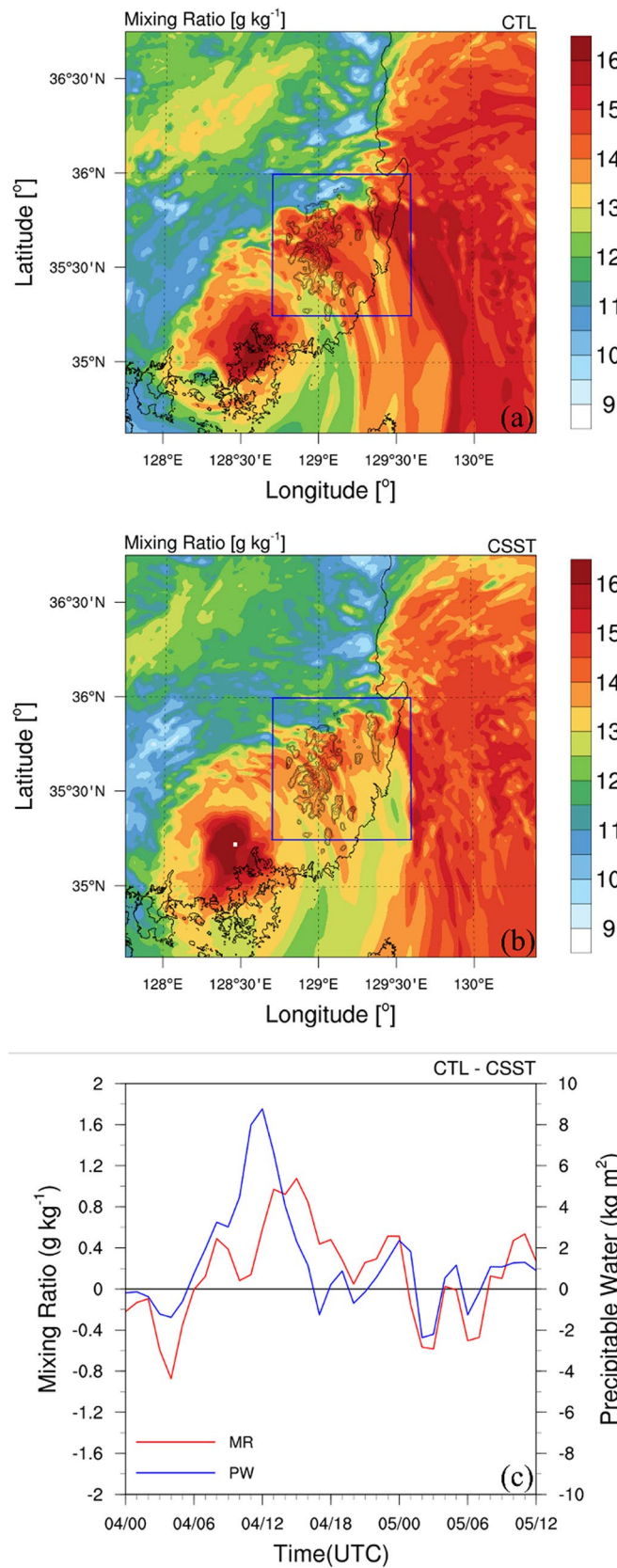


**Fig. 11** (See legend on previous page.)



## Supplementary Information

The online version contains supplementary material available at <https://doi.org/10.1186/s40562-022-00230-1>.

**Additional file 1: Figure S1.** SST linear regression of Sep and Oct using monthly OISST data for 37 years (1982–2018). The hatched areas are above the 95% confidence level. **Figure S2.** 37-yr annual variation of sea surface temperature of East China Sea during Oct 1 to Oct 5. The solid black line is the SST using OISST daily production, and the solid blue line is the detrended SST of OISST. The black, red, and blue dashed lines are the mean SST of OISST, one standard deviation of OISST, and one standard deviation of detrended SST, respectively.

### Acknowledgements

The authors appreciate the provision of computing resources and support by the Republic of Korea Airforce and the Ulsan National Institute of Science and Technology.

### Author contributions

WC proposed the subject of this paper and wrote the manuscript. D-HC, JP, JM, and YP revised the manuscript. H-SK, KN, and S-HP contributed to model integration and provided computing resources. All authors read and approved the final manuscript.

### Funding

This work was partially funded by the Ulsan National Institute of Science and Technology [Grant No. 1.220031.01], and the 2021 Republic of Korea Airforce Numerical Weather Prediction Research and Development Program, the development of Numerical Weather Prediction and Data Application Techniques.

### Availability of data and materials

Not applicable.

### Declarations

#### Competing interests

The authors declare that they have no competing interests.

#### Author details

<sup>1</sup>Department of Urban and Environmental Engineering, Ulsan National Institute of Science and Technology, 50 UNIST-gil, Ulsu-gun, Ulsan 689-798, Republic of Korea. <sup>2</sup>Department of Atmospheric Sciences, University of Washington, Seattle, WA, USA. <sup>3</sup>Weather Unit, 10th Fighter Wing, Republic of Korea Airforce, Gyeryong, South Korea.

Received: 17 September 2021 Accepted: 2 May 2022

Published online: 17 August 2022

### References

- Agyakwah W, Lin Y-L (2021) Generation and enhancement mechanisms for extreme orographic rainfall associated with Typhoon Morakot (2009) over the Central Mountain Range of Taiwan. *Atmos Res* 247:105160
- Chiao S, Lin Y-L (2003) Numerical modeling of an orographically enhanced precipitation event associated with Tropical Storm Rachel over Taiwan. *Weather Forecast* 18(2):325–344
- Chu C-M, Lin Y-L (2000) Effects of orography on the generation and propagation of mesoscale convective systems in a two-dimensional conditionally unstable flow. *J Atmos Sci* 57(23):3817–3837
- Do G, Kim H-S (2021) Effect of mid-latitude jet stream on the intensity of tropical cyclones affecting Korea: observational analysis and implication from the numerical model experiments of Typhoon Chaba (2016). *Atmosphere* 12(8):1061
- Emanuel K (2005) Increasing destructiveness of tropical cyclones over the past 30 years. *Nature* 436(7051):686–688
- Hong SY (2010) A new stable boundary-layer mixing scheme and its impact on the simulated East Asian summer monsoon. *Q J R Meteorol Soc* 136(651):1481–1496
- Hong S-Y, Noh Y, Dudhia J (2006) A new vertical diffusion package with an explicit treatment of entrainment processes. *Mon Weather Rev* 134(9):2318–2341
- Huang Y-C, Lin Y-L (2014) A study on the structure and precipitation of Morakot (2009) induced by the Central Mountain Range of Taiwan. *Meteorol Atmos Phys* 123(3):115–141
- Jang SM, Yoon SK, Park KW Verification of initial field of very short-term radar rainfall forecasts using advanced system: A case study of Typhoon CHABA in 2016. In: Proceedings of the Korea Water Resources Association Conference, Korea Water Resources Association, 2018. pp 100–100
- Kain JS (2004) The Kain-Fritsch convective parameterization: an update. *J Appl Meteorol* 43(1):170–181
- Kain JS, Fritsch JM (1990) A one-dimensional entraining/detraining plume model and its application in convective parameterization. *J Atmos Sci* 47(23):2784–2802
- Kain JS, Baldwin ME, Weiss SJ (2003) Parameterized updraft mass flux as a predictor of convective intensity. *Weather Forecast* 18(1):106–116
- Kanada S, Tsujino S, Aiki H, Yoshioka MK, Miyazawa Y, Tsuboki K, Takayabu I (2017) Impacts of SST patterns on rapid intensification of Typhoon Megi (2010). *J Geophys Res Atmos* 122(24):13245–13262
- Kim S-J, Woo S-H, Kim B-M, Hur S-D (2011) Trends in sea surface temperature (SST) change near the Korean peninsula for the past 130 years. *Ocean Polar Res* 33(3):281–290
- Kim H, Heo K-Y, Kwon J-I, Park K-S (2018) Simulation of Typhoon Chaba over Korean Peninsula using HWRF Modeling System. *J Coast Res* 85(10085):751–755
- Kumar BP, Cronin MF, Joseph S, Ravichandran M, Sureshkumar N (2017) Latent heat flux sensitivity to sea surface temperature: regional perspectives. *J Clim* 30(1):129–143
- Lee J-H, Lim B-J, Kim D-Y, Park S-H, Chang Y-S (2018a) The validation of MOHID regional ocean circulation model around the East Asian Seas in 2016. *J Korean Earth Sci Soc* 39(5):436–457
- Lee J-T, Ko K-Y, Lee D-I, You C-H, Liou Y-C (2018b) Enhancement of orographic precipitation in Jeju Island during the passage of Typhoon Khanun (2012). *Atmos Res* 201:58–71
- Lee M, Cha DH, Moon J, Park J, Jin CS, Chan JC (2019) Long-term trends in tropical cyclone tracks around Korea and Japan in late summer and early fall. *Atmos Sci Lett* 20(11):e939
- Li DY, Huang CY (2018) The influences of orography and ocean on track of Typhoon Megi (2016) past Taiwan as identified by HWRF. *J Geophys Res Atmos* 123(20):11492–11517
- Lin Y-L (2007) *Mesoscale dynamics*, vol 630. Cambridge University Press, Cambridge
- Lin Y-L, Chiao S, Wang T-A, Kaplan ML, Weglarz RP (2001) Some common ingredients for heavy orographic rainfall. *Weather Forecast* 16(6):633–660
- Lin Y, Zhao M, Zhang M (2015) Tropical cyclone rainfall area controlled by relative sea surface temperature. *Nat Commun* 6(1):1–7
- Liu Q, Zhang Q (2013) Analysis on long-term change of sea surface temperature in the China Seas. *J Ocean Univ China* 12(2):295–300
- Milbrandt J, Morrison H (2016) Parameterization of cloud microphysics based on the prediction of bulk ice particle properties. Part III: introduction of multiple free categories. *J Atmos Sci* 73(3):975–995
- Ming-Jen Y, Lin C (2005) A modeling study of Typhoon Toraji (2001): physical parameterization sensitivity and topographic effect. *TAO Terr Atmos Ocean Sci* 16(1):177
- Moon J, Cha DH, Lee M, Kim J (2018) Impact of spectral nudging on real-time tropical cyclone forecast. *J Geophys Res Atmos* 123(22):12647–12660
- Morrison H, Milbrandt JA (2015) Parameterization of cloud microphysics based on the prediction of bulk ice particle properties. Part I: scheme description and idealized tests. *J Atmos Sci* 72(1):287–311
- Morrison H, Milbrandt JA, Bryan GH, Ikeda K, Tessorndorf SA, Thompson G (2015) Parameterization of cloud microphysics based on the prediction of bulk ice particle properties. Part II: case study comparisons with observations and other schemes. *J Atmos Sci* 72(1):312–339

- Park DSR, Ho CH, Kim JH, Kim HS (2011) Strong landfall typhoons in Korea and Japan in a recent decade. *J Geophys Res Atmos*. <https://doi.org/10.1029/2010JD014801>
- Rostom R (2015) Effects of orography on track continuity of cyclones and precipitation associated with tropical cyclones passing over the Southern-Central Appalachian Mountains. Ph.D. Diss., North Carolina Agricultural and Technical State University
- Sun Y, Zhong Z, Li T, Yi L, Hu Y, Wan H, Chen H, Liao Q, Ma C, Li Q (2017) Impact of ocean warming on tropical cyclone size and its destructiveness. *Sci Rep* 7(1):1–10
- Tang CK, Chan JC (2014) Idealized simulations of the effect of Taiwan and Philippines topographies on tropical cyclone tracks. *Q J R Meteorol Soc* 140(682):1578–1589
- Tao D, Zhang F (2014) Effect of environmental shear, sea-surface temperature, and ambient moisture on the formation and predictability of tropical cyclones: an ensemble-mean perspective. *J Adv Model Earth Syst* 6(2):384–404
- von Storch H, Langenberg H, Feser F (2000) A spectral nudging technique for dynamical downscaling purposes. *Mon Weather Rev* 128(10):3664–3673
- Webster PJ, Holland GJ, Curry JA, Chang H-R (2005) Changes in tropical cyclone number, duration, and intensity in a warming environment. *Science* 309(5742):1844–1846
- Witcraft NC, Yuh-Lang L, Kuo Y-H (2005) Dynamics of orographic rain associated with the passage of a tropical cyclone over a mesoscale mountain. *TAO Terr Atmos Ocean Sci* 16(5):1133
- Yang M-J, Zhang D-L, Huang H-L (2008) A modeling study of Typhoon Nari (2001) at landfall. Part I: topographic effects. *J Atmos Sci* 65(10):3095–3115
- Yuk J-H, Joh M (2019) Prediction of typhoon-induced storm surge, waves and coastal inundation in the Suyeong River Area, South Korea: a case study during typhoon Chaba. *J Coast Res* 91(SI):156–160

## Publisher's Note

Springer Nature remains neutral with regard to jurisdictional claims in published maps and institutional affiliations.

Submit your manuscript to a SpringerOpen<sup>®</sup> journal and benefit from:

- ▶ Convenient online submission
- ▶ Rigorous peer review
- ▶ Open access: articles freely available online
- ▶ High visibility within the field
- ▶ Retaining the copyright to your article

---

Submit your next manuscript at ▶ [springeropen.com](https://www.springeropen.com)

---